THE JOURNAL OF PHYSICAL CHEMISTRY B

Article

pubs.acs.org/JPCB

Disentangling Electron Tunneling and Protein Dynamics of Cytochrome *c* through a Rationally Designed Surface Mutation

Damián Alvarez-Paggi,[†,⊥] Wiebke Meister,[‡,⊥] Uwe Kuhlmann,[‡] Inez Weidinger,[‡] Katalin Tenger,[§] László Zimányi,[§] Gábor Rákhely,[¶] Peter Hildebrandt,*[,‡] and Daniel H. Murgida*[,†]

[†]INQUIMAE-CONICET and Departamento de Química Inorgánica, Analítica y Química Física, Facultad de Ciencias Exactas y Naturales, Universidad de Buenos Aires, Ciudad Universitaria, pab. 2, piso 3, C1428EHA-Buenos Aires, Argentina

[‡]Institut für Chemie, Technische Universität Berlin, Strasse des 17. Juni 135, Sekr. PC14, D-10623-Berlin, Germany

[§]Biological Research Center, Institute of Biophysics, H-6726 Szeged, Temesvári krt. 62, Hungary

[¶]Department of Biotechnology, University of Szeged, H-6726, Közép fasor 52, Hungary

Supporting Information

ABSTRACT: Nonexponential distance dependence of the apparent electron-transfer (ET) rate has been reported for a variety of redox proteins immobilized on biocompatible electrodes, thus posing a physicochemical challenge of possible physiological relevance. We have recently proposed that this behavior may arise not only from the structural and dynamical complexity of the redox proteins but also from their interplay with strong electric fields present in the experimental setups and in vivo (*J. Am Chem. Soc.* **2010**, *132*, 5769−5778). Therefore, protein dynamics are finely controlled by the energetics of both specific contacts and the interaction between the protein's dipole moment and the interfacial electric fields. In turn, protein dynamics may govern electron-transfer kinetics through reorientation from low to high donor−acceptor electronic coupling orientations. Here we present a combined computational and experimental study of WT cytochrome *c* and the surface mutant K87C adsorbed on electrodes coated with self-assembled monolayers (SAMs) of varying thickness (i.e., variable strength of the interfacial electric field). Replacement of the positively charged K87 by a neutral amino acid allowed us to disentangle protein dynamics and electron tunneling from the reaction kinetics and to rationalize the anomalous distance dependence in terms of (at least) two populations of distinct average electronic couplings. Thus, it was possible to recover the exponential distance dependence expected from ET theory. These results pave the way for gaining further insight into the parameters that control protein electron transfer.

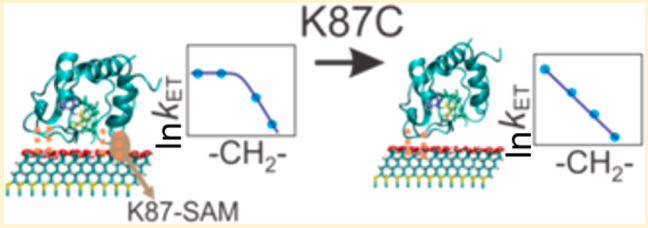

INTRODUCTION

Electron-transfer (ET) proteins present a structural and dynamical complexity that pose several challenges to the well-established theoretical frame of (bio)electrochemistry. For instance, the reigning theory of long-range redox reactions predicts an exponential decay of the ET rate constants with the distance between electron donor and acceptor that has been readily verified for a large number of experimental systems.[1] However, such dependency breaks down for several different ET proteins adsorbed on electrodes coated with self-assembled monolayers (SAMs) of variable chain length.[2−11] These phenomena have spurred an active research field while hinting at a possible role in the regulation of ET reactions in vivo.

We have recently proposed a mechanism involving electric-field-controlled protein reorientation to rationalize the anomalous distance dependence of k_{ET} for cytochrome *c* (Cyt) electrostatically adsorbed on SAMs of carboxyl-terminated alkanethiols and related systems.[6,12] Using molecular dynamics (MD) simulations, it was shown that Cyt may interact electrostatically with the COOH-terminated SAMs through four different protein surface regions, thus leading to a distribution of orientations.[12] This distribution, however, is relatively narrow as one of the regions that has been designated as the interaction main zone (MZ) exhibits significantly higher binding energies and a largely perpendicular orientation of the dipole moment of the protein with respect to the surface. The electrostatic contacts of the MZ with the SAM involve lysine residues 13, 72, 73, 79, 86, and 87 for both ferric and ferrous Cyt, thus resulting in a heme group oriented roughly perpendicular with respect to the surface and with its exposed edge in direct contact with the SAM. In addition to the above-mentioned residues, ferrous Cyt exhibits further contacts with the SAM through lysines 22, 25, and 27, which force the heme into a more perpendicular orientation compared with the ferric form (125°). Remarkably, altogether the same residues have been implicated in the interactions of Cyt with natural redox partners such as cytochrome *c* oxidase, cytochrome *c* peroxidase, and the bc_1 complex.[12−15]

Received: January 24, 2013
Revised: April 5, 2013
Published: April 23, 2013

dx.doi.org/10.1021/jp400832m | *J. Phys. Chem. B* 2013, 117, 6061−6068

Pathways analysis shows that the preferred orientation of ferrous Cyt in electrostatic complexes leads to nearly optimal electronic coupling with the SAM-coated metal. In contrast, the most favorable orientation of ferric Cyt establishes a relatively weak electronic coupling, thus requiring transient protein reorientation as a prerequisite for fast heterogeneous ET. This gating step, in turn, is predicted to be controlled by the charge density of the SAM and by the interfacial electric field.[12] In agreement with these computational results, time-resolved surface-enhanced resonance Raman (TR-SERR) spectroelectrochemical experiments demonstrated that, for thick SAMs, corresponding to weak electric fields, reorientation is much faster than electron transfer, whereas for thinner films (stronger fields) both processes occur at the same rate, thus suggesting reorientation as the rate-limiting event.[6]

Establishing the validity of this hypothesis unambiguously is motivated by its implications for both fundamental and applied science. The electric field control of protein dynamics in electrostatic complexes might constitute the basis of a general feedback mechanism for the regulation of electron−proton energy transduction in respiration and photosynthesis exerted by variations of the membrane potential.[12,16−19] Moreover, it may afford a consistent explanation to the unusual distance dependences of k_{ET} often observed in bioelectrochemistry,[2−11] thereby inspiring new strategies for the development of efficient bioelectronic devices.[20,21]

The present work is dedicated to further test the above-mentioned hypothesis both experimentally and theoretically by altering protein binding, dynamics, and electronic coupling through a surface mutation. Careful inspection of our previous results reveals six key lysine residues that may be crucial in determining interfacial ET.[12] Among them, K87 is particularly interesting as replacement of this residue by a neutral amino acid would in principle abolish contacts that stabilize low electronic coupling orientations. Indeed, MD simulations and pathways calculations reported here for the in silico K87C mutant predict an enhanced average electronic coupling for this protein variant, thus constituting a rational choice for experimental studies. Therefore, we have produced the K87C variant and studied its heterogeneous ET reaction in protein/SAM electrostatic complexes. Time-resolved surface-enhanced resonance Raman (TR-SERR) spectroelectrochemical experiments show an excellent agreement with the theoretical predictions, thus unveiling the role of protein dynamics behind the anomalous distance dependences in biological ET reactions.

EXPERIMENTAL SECTION

Chemicals. 6-Mercaptohexanoic acid (C5) was purchased from Dojindo. All other chemicals including 11-mercaptoundecanoic acid (C10) and 16-mercaptohexadecanoic acid (C15) were purchased from Sigma-Aldrich and used without further purification. Horse heart cytochrome *c* (Cyt) was obtained from Sigma-Aldrich and purified by HPLC. The water used in all experiments was purified by a Millipore system and its resistance was greater than 18 MΩ.

Protein Expression and Purification. The K87C mutant of horse heart cytochrome *c* was produced by site-directed mutagenesis and coexpression with the yeast cytochrome *c* heme lyase in the BL21-AI (Invitrogen) *E. coli* strain, according to procedures previously described.[22,23] The genes of the mutant cytochrome *c* and heme lyase were cloned into the arabinose-inducible pBAD24 plasmid. The successful mutation of the cytochrome gene has been verified by sequencing. The mutant cytochrome *c* protein was purified on a CM-Sephadex C50 cation exchange matrix. The purity was confirmed by UV−visible spectroscopy as well as SDS-gel electrophoresis. Protein stability was confirmed by UV−visible and resonance Raman (RR) spectroscopy, as the spectra are identical to those of Cyt WT, and supported by the preserved folding obtained by MD calculations.

Surface-Enhanced Resonance Raman and Resonance Raman Spectroscopy. Silver ring electrodes were mechanically polished with 3 M polishing films from 30 to 1 μm grade. After washing and sonication in water and ethanol, electrodes were subjected to several oxidation−reduction cycles in 0.1 M KCl to create a SER-active nanostructured surface. Subsequently, the electrodes were incubated in about 1.5 mM ethanolic solutions of the alkanethiol for ca. 20 h, and then rinsed and transferred to the spectroelectrochemical cell. For electrostatic adsorption Cyt was added to the electrochemical cell from a stock solution to a final concentration of 0.2−0.4 μM in 30 mM phosphate buffer at pH 7.0 and allowed to incubate at room temperature 30−60 min at −100 mV (vs Ag/AgCl (3 M KCl)) before starting the experiments. In the case of the K87C mutant, covalent binding to the metal electrode through the cysteine group can be discarded as washing of the electrodes with high ionic strength buffer leads to complete desorption of the protein.

The spectroelectrochemical cell for SERR spectroscopy has been described elsewhere.[24] Briefly, a Pt wire and a Ag/AgCl electrode were used as counter and reference electrodes, respectively. All reported potentials in this work refer to the Ag/AgCl (3 M KCl) electrode. The working electrode was a silver ring of 8 mm diameter and 2.5 mm height mounted on a shaft that is rotated at about 5 Hz to avoid laser-induced sample degradation. As electrolyte solution a 30 mM phosphate buffer, pH 7.0, was used.

SERR spectra were measured in backscattering geometry by using a confocal microscope coupled to a single-stage spectrograph (Jobin Yvon, LabRam 800 HR or XY 800) equipped with a liquid-nitrogen-cooled back-illuminated CCD detector. Elastic scattering was rejected with notch or edge filters. The 413 nm line of a CW krypton ion laser (Coherent Innova 300c) was focused onto the surface of the rotating Ag electrode by means of a long-working-distance objective (Nikon 20x, N.A. 0.35) with a working distance of 20 mm. Typically, experiments were performed with laser powers of about 1 mW at the sample. Effective acquisition times were between 3 and 10 s. All experiments were repeated several times to ensure reproducibility. For the determination of the redox equilibria, stationary spectra at different fixed potentials were measured in the potential range from −400 to +150 mV. For TR-SERR experiments, potential jumps of variable height and duration were applied to trigger the reaction. The SERR spectra were measured at different delay times following the potential jump. Synchronization of potential jumps and probe laser pulses was achieved by a home-built pulse-delay generator. The probe pulses were generated by passing the CW laser beam through two consecutive laser intensity modulators (Linos), which give a total extinction better than 1:50 000 and a time response of ca. 20 ns. Details of the TR-SERR measurements are described elsewhere.[8] After background subtraction the spectra were treated by component analysis[25] in which the spectra of the individual species were fitted to the measured spectra by using homemade analysis software based on Matlab software. The time-dependent spectral changes were converted

dx.doi.org/10.1021/jp400832m | J. Phys. Chem. B 2013, 117, 6061−6068

into changes of the relative concentrations of the species involved and subsequently analyzed in terms of relaxation kinetics to yield reciprocal relaxation time constants.[8]

The integrity of the SAM coating was checked both before protein adsorption and after experimental determinations by SER under 514 nm excitation. Inspection of the C−S vibrational stretching mode indicated the dominant contribution of *trans* conformers of the alkanethiol chain, indicative of well-ordered compact SAMs.[26]

Computational Methods. The initial structure of ferric Cyt was obtained from the PDB database (1HRC).[27] The computational methods have been described in detail previously.[12] Briefly, MD simulations were performed using the AMBER 2005 package, with the f99 force field implementation and heme parameters adopted from previous work. To simulate the SAMs, an infinite array of fixed Au atoms with lattice structure 111 was built in silico. Each of the Au atoms was linked to a HS−$(CH_2)_5$−COOH molecule (C_5) through the S atom. SAM and lattice parameters were adopted from the literature.[28] Adsorption of Cyt to C_5-SAMs was investigated using steered MD simulations (SMD) starting from 26 different configurations that differ solely in the rotational orientation of the protein with respect to the SAM. For each starting configuration, Cyt was pulled toward the surface at constant velocity, while computing the applied force. The pulling reaction coordinate (RC) is defined as the distance between the fixed central Au atom and the center of mass of the C^{α} atoms of the protein. Integration of the force applied for moving the protein toward the surface yields the work performed along the RC. From the 26 starting orientations that extensively sample possible Cyt/SAM complex structures, those showing a minimum in the work-versus-RC profiles at contact distances were selected as stable electrostatic complexes and each subjected to 20 ns periodic boundary conditions (PBC) simulations in explicit TIP3P water molecules. From these simulations, binding energies were estimated using molecular mechanics/generalized Born surface area (MM/GBSA), while the electronic coupling matrix elements were calculated using the pathways algorithm developed by Beratan et al.[29] The orientation of Cyt with respect to the Au/SAM surface is defined by the relative heme orientation using two angles, α and φ (Scheme 1 and Scheme S1 in the Supporting Information). α is defined as the angle between the heme plane and the surface. Thus, values of α close to 0° or 180° imply that the heme lies parallel to the SAM, whereas values close to 90° indicate a perpendicularly oriented heme. φ is defined by the Fe−N_A bond and the vector pointing toward the SAM which lies in the heme plane, and describes the rotational orientation of the protein. Values of φ between 0° and 90° correspond to protein orientations with the heme propionates pointing toward the SAM, whereas for values in the range 180°-270° the propionates point in the opposite direction.

Note that, for α values close to 0° or to 180°, changes of φ do not correspond to significant variations of protein orientation since the heme remains parallel to the SAM surface.

The protein dipole moment was computed with respect to the center of charge of the protein, as reported by Margoliash et al.,[30] and its relative orientation is defined as the angle between the dipole vector and the *Z* axis normal to the SAM plane.

In order to improve sampling of the possible Cyt−SAM complexes for the K87C mutant, three additional 20 ns MD simulations were performed with starting orientations adapted from those found in our previous work for WT Cyt.[12]

Scheme 1. Representation of the Rotational Angles α (left) and φ (right)

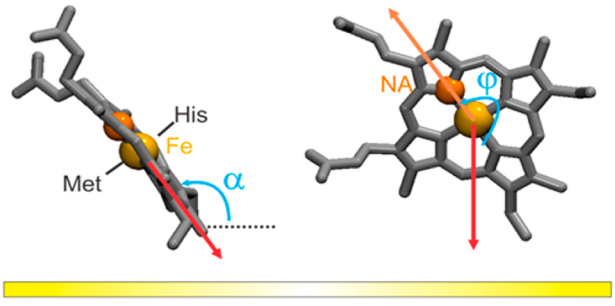

RESULTS AND DISCUSSION

MD Characterization of the K87C Cyt Mutant in Electrostatic Complexes. Previous experimental and computational studies of WT Cyt electrostatically adsorbed on SAM-coated electrodes indicate that heterogeneous ET dynamics in these complexes is largely determined by protein reorientation.[6,12] To further test this hypothesis, we considered abolishing key Cyt−SAM contacts that stabilize low coupling orientations, while preserving the average coarse orientation. The results obtained from our previous MD simulations[12,31] suggest that contacts involving lysines 72 and 73 are ubiquitous in Cyt−SAM complexes. In addition, lysines 22 and 25 stabilize orientations with high electronic coupling, while lysines 86 and 87 participate in orientations that yield a low electronic coupling. These results suggest lysine 87 (K87) as a good candidate for being replaced by a neutral residue for this purpose (Figure S1 in the Supporting Information). Therefore, the K87C variant of ferric Cyt was created in silico by replacement of the corresponding amino acid in the PDBID 1HRC structure,[27] followed by 10 ns thermalization. Root-mean-square deviations (rmsd) of the backbone atoms of the mutant from the reference structure remained largely constant along the simulation, with an average value of 1.5 Å (Figure S2 in the Supporting Information), suggestive of a well preserved and stable native folding.

Adsorption of K87C on electrodes coated with C5-SAMs was investigated by SMD simulations following the procedures described previously.[12] Briefly, we computed work-versus-distance profiles obtained by pulling the protein toward the SAM, starting from 26 different orientations that span a comprehensive range of possible Cyt−SAM complexes. Five of these orientations resulted in protein binding, as determined by the appearance of minima at contact distances in the profiles (Figure S3 in the Supporting Information). The dynamics of Cyt in these five stable complexes was explored by performing 20 ns MD simulations in explicit solvent for each starting orientation. RMSD values of the adsorbed K87C from the initial structure remained below 2.5 Å along the simulations (Figure S4 in the Supporting Information), thereby indicating that the native folding is preserved.

Figure 1 summarizes the orientations explored by K87C along the different 20 ns simulations starting from the five initial K87C/SAM structures identified by SMD as stable electrostatic complexes. The protein orientation is represented in terms of the angles α and φ as defined in Scheme S1, with constant φ values indicated as dotted isolines.

dx.doi.org/10.1021/jp400832m | J. Phys. Chem. B 2013, 117, 6061−6068

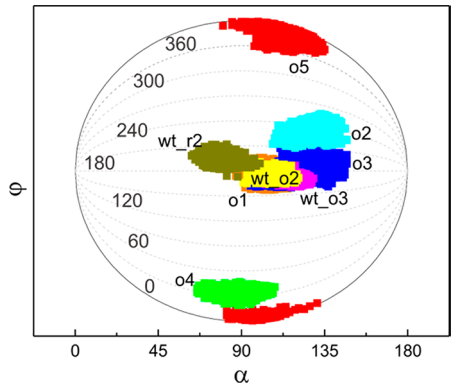

Figure 1. Conformations of the K87C^{3+}−SAM complex defined by the orientational angles α and φ obtained from all equilibrium MD simulations in explicit solvent. Each point represents a snapshot from the corresponding MD, which are represented in different colors. Snapshots were taken every 10 ps. "wt" refers to starting orientations adopted from Cyt WT either in the oxidized (o) or reduced (r) state.[12] The dotted lines represent isovalues of φ. For a description of the lysine residues that establish Cyt−SAM contacts in each orientation see Figure S1 in the Supporting Information.

The complexes denoted as o4 and o5 present φ values close to 0° or to 360°, while for o2 this value is close to 240°, implying that in these three cases the partially exposed heme edge remains apart from the SAM surface. As the electronic coupling decays exponentially with distance, the k_{ET} from these orientations would be orders of magnitude slower and not experimentally detectable under conditions that allow for the detection of well oriented molecules. In addition, binding energies from these complexes are small (Figure S3). Altogether, these results render direct ET from these orientations quite unlikely. Therefore, these structures are regarded as not relevant for the reaction and were not considered further. For the remaining initial complexes (o1, o3) the protein explores the central region shown in Figure 1, which corresponds to a heme group perpendicularly oriented and in close contact to the SAM such that, a priori, they can be regarded as electrochemically competent. In order to improve sampling of this region, we also performed 20 ns MD simulations of K87C using three additional starting complexes that were adopted from previous work[12] and correspond to regions of high electronic coupling found for ferrous (wt_r2) and ferric (wt_o2, wt_o3) wild-type Cyt.

The regions explored in the latter five dynamics (wt_o2, wt_o3, wt_r2, o1, o3) present significant overlap and, taken together, constitute the main zone (MZ) to be considered for analyzing protein and ET dynamics.

Figure 2 compares the MZ explored by the K87C mutant obtained in the present work with that found previously for WT Cyt.[12] Note that K87C explores a broader range of α angles and, in average, presents slightly higher φ values and lower α values.

The data in Figure 2 are presented employing a color code that represents a scale of binding free energies obtained by the MM/GBSA method. In the MZ, these energies vary between −30 and −60 kcal mol^{-1} for K87C, whereas for the WT protein they cover the range from −30 to −110 kcal mol^{-1}. Thus, simulations predict that, upon abolishing the K87−SAM electrostatic contact, the protein exhibits weaker binding and is able to explore a broader range of orientations with respect to the electrode surface.

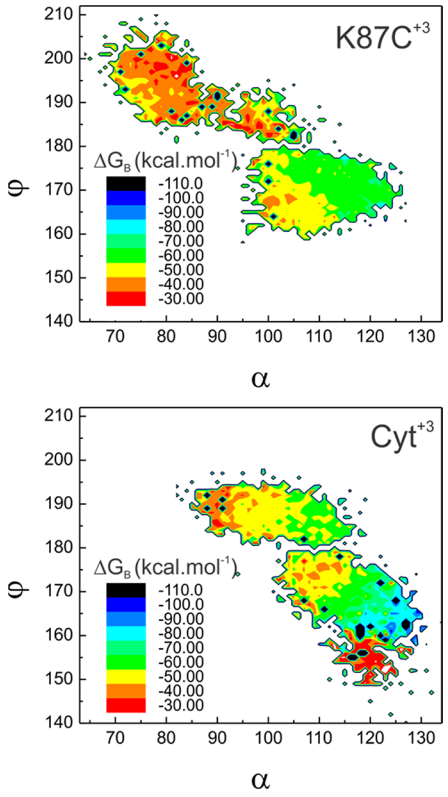

Figure 2. Binding energies as a function of the orientational angles for the MZ orientations of ferric K87C (top panel) and WT (bottom panel) Cyt variants. The color code indicates increasing binding energies from −110 kcal mol^{-1} (black) to −30 kcal mol^{-1} (red).

Pathways Analysis of the Protein/SAM Complexes. The electronic matrix elements of the protein/SAM electrostatic complexes were evaluated semiquantitatively by employing the pathways algorithm.[29] To that end, electronic coupling decays (D^H) between the heme iron and the metal surface were calculated for K87C and WT Cyt along the five 20 ns trajectories that define the MZ represented in Figure 2. The results are summarized in Figure 3 in terms of the orientational angles α and φ.

The stronger electronic couplings are achieved for protein orientations with $\alpha < 95°$, which are only explored by the K87C mutant, thus suggesting faster heterogeneous ET for this variant. Note that coupling decays adopt values between 7×10^{-4} and 8×10^{-4} for $\alpha < 95°$ and between 2×10^{-4} and 3×10^{-4} for $\alpha > 95°$. Therefore, ET of K87C in the low-affinity orientations ($\alpha < 95°$) is predicted to be between 16 and 36 times faster than in the high-affinity orientations ($\alpha > 95°$). Evaluation of the protein dipole moment in the adsorbed state as a function of the orientation shows that the modulus is not significantly affected upon mutation (Figure S5 in the Supporting Information). However, while WT Cyt does not exhibit a preferential orientation for dipole alignment with the vector normal to the surface, i.e., with the interfacial electric field,[12] K87C presents better alignment in the low-affinity orientations.

In summary, MD simulations and pathways calculations predict that replacement of Lys87 by a neutral amino acid should exert a strong impact on the interplay of protein dynamics and electronic coupling of Cyt in electrostatic complexes. Therefore, we produced the K87C mutant and investigated its heterogeneous ET dynamics experimentally.

dx.doi.org/10.1021/jp400832m | J. Phys. Chem. B 2013, 117, 6061−6068

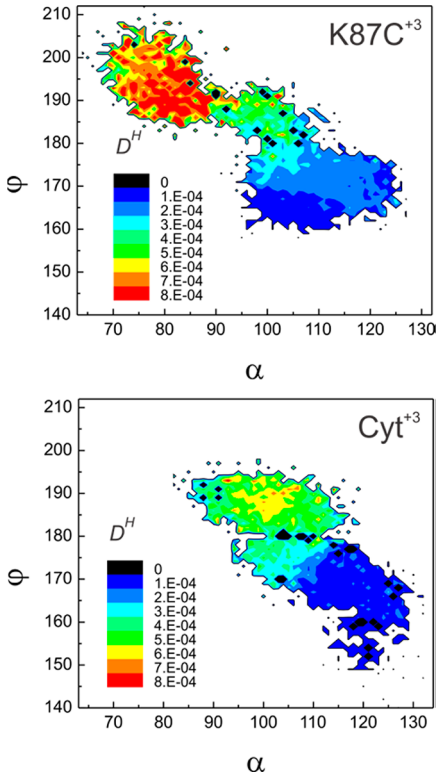

Figure 3. Average electronic coupling decays as a function of the orientational angles for the MZ orientations of ferric K87C (top panel) and WT (bottom panel) Cyt variants. The color code indicates increasing electronic coupling decays, from 1×10^{-4} (blue) to 8×10^{-4} (red).

Structural and Redox Equilibria of the Immobilized Proteins. WT Cyt and the single mutant K87C were electrostatically adsorbed on nanostructured Ag electrodes coated with SAMs of HS−$(CH_2)_n$−COOH with n = 5, 10, and 15 (C5, C10, and C15, respectively). The structure of the adsorbed proteins at the level of the redox sites was monitored by SERR spectroelectrochemistry under Soret-band excitation with 413 nm. In agreement with previous reports,[8,24,32] SERR spectra of WT Cyt adsorbed on C10 and C15 SAMs recorded at oxidizing and reducing potentials are essentially identical to the resonance Raman (RR) spectra of the chemically oxidized and reduced native protein in solution, respectively, thus indicating a conserved heme pocket structure (Figure S6 in the Supporting Information). Moreover, SERR spectra recorded at different electrode potentials could be quantitatively simulated by superposition of the RR spectra of native Cyt (also called B1 state) with variable contributions of the ferrous and ferric forms (Figure S7 in the Supporting Information). Only for very positive electrode potentials, the component analysis of the SERR spectra reveals minor contributions of the so-called B2 species of Cyt,[32] in which the axial ligand Met80 is displaced from the heme iron, resulting in a five-coordinated high-spin heme species (B2oxHS) in equilibrium with a non-native six-coordinate low-spin form (B2oxLS) with a His residue bound to the sixth axial position (Figure S8 in the Supporting Information). The structural transition to the B2 state is only observed for the ferric protein, whereas upon electrochemical reduction the B1 form is fully recovered.

Similar results were obtained for the K87C mutant, except that in this case the amounts of B2 species can reach total spectral contributions of up to 20% (Figure S8) which, as for the WT protein, remain constant within the time window of the experiments. Component analysis of the potential-dependent SERR spectra for both protein variants on the different SAMs affords nearly ideal Nernst plots (Figure S9 in the Supporting Information) with reduction potentials close to 20 mV for the corresponding B1 states (Table 1), i.e., very similar to the native protein in solution.[33]

Electron-Transfer Dynamics. The kinetics of heterogeneous ET of the protein/SAM electrostatic complexes was investigated by TR-SERR spectroelectrochemistry. In these experiments the redox equilibrium of immobilized Cyt is perturbed by applying steps from an initial (E_i) to a final (E_f) electrode potential, while recording SERR spectra at variable delay times along the perturbation. Two types of experiments were performed for both protein variants: (i) in the oxidative direction at nearly zero driving force with E_i = −80 mV and E_f = 20 mV ($\cong E^0$) and (ii) in the reductive direction from E_i = 40 mV to E_f = −200 mV, corresponding to a ca. −220 mV overpotential for the ET reaction. In all cases TR-SERR spectra could be quantitatively reproduced using variable contributions of the same spectral components found in stationary experiments, i.e., the ferrous and ferric (native) state B1 of Cyt and additional small contributions from the B2oxHS and B2oxLS species. As the reduction potentials of the B2 species are below −300 mV,[32] these species do not undergo redox chemistry within the potential windows of the experiments and, moreover, their spectral contributions remained invariant. Typical TR-SERR spectra obtained for K87C are shown in Figure 4, along with the corresponding spectral components.

The spectral component contributions were converted into relative surface concentrations by employing relative reciprocal cross sections determined previously.[34] Time−concentration profiles obtained from this analysis for the B1 state of WT Cyt adsorbed on the various SAMs can be well described as one-step relaxation processes (Figure 5A), characterized by apparent ET rate constants (k_{ET}^{app}) very close to values reported previously for comparable experimental conditions (Table 1).[6]

Table 1. Thermodynamic (E^0) and Kinetic (k_{ET}^{app}) Values for Cyt WT and K87C Determined by TR-SERR for Protein Samples Adsorbed on C5, C10 and C15 SAMs[a]

	WT			K87C		
		k_{ET}^{app} (s^{-1})			k_{ET}^{app} (s^{-1})	
	E^0 (mV)	−80 → +20 mV	+40 → −200 mV	E^0 (mV)	−80 → +20 mV	+40 → −200 mV
C5	19	308 ± 20	735 ± 80	23	317 ± 17	1185 ± 120
C10	20	45 ± 4	221 ± 69	20	238 ± 146/11 ± 7	858 ± 235/32 ± 15
C15	21	0.3 ± 0.2	1.2 ± 0.35	13	5.2 ± 0.3/0.3 ± 0.2	9 ± 7/0.40 ± 0.35

[a]The potential step applied is indicated in each case.

dx.doi.org/10.1021/jp400832m | J. Phys. Chem. B 2013, 117, 6061−6068

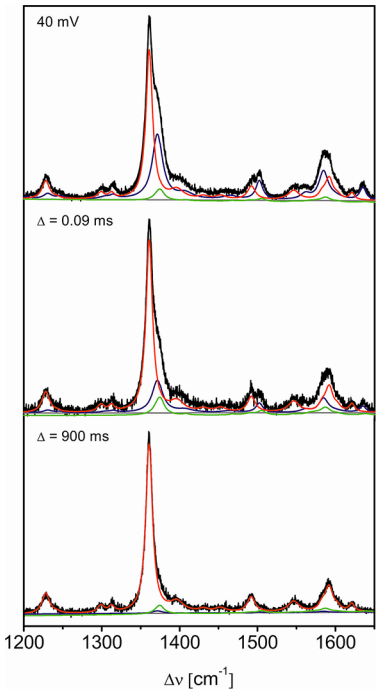

Figure 4. SERR and TR-SERR spectra of K87C immobilized on an Ag electrode coated by a C10-SAM, measured with 413 nm excitation, prior to a potential jump from 40 mV (top) to −200 mV after delay times of 0.09 ms (middle) and 900 ms (bottom). The component spectra of the ferrous B1, ferric B1, and the ferric B2 (HS and LS) states are represented by red, blue, and green lines, respectively.

Monophasic heterogeneous ET kinetics was also observed for the K87C protein adsorbed on C5 SAMs, with k_{ET}^{app} very similar to those determined for the WT protein at equivalent chain lengths and overpotentials.

In sharp contrast, however, time traces recorded for K87C adsorbed on C10 and C15 SAMs exhibit reproducible biphasic kinetics (Figure 5 and Table 1). Partial protein dimerization through sulfur bridge formation between cysteine residues is ruled out as it is not observed for C5 SAMs and, on the other hand, TR-SERR experiments performed with K87C freshly reduced with tris(2-carboxyethyl)phosphine[35] yield identical results.

For both reduction and oxidation, when considering the fast kinetic component of K87C from C10 and C15 along with the single component from C5, the observed distance dependence is characterized by an exponential variation of k_{ET}^{app} at the thicker films, followed by a plateau at thinner films (Figure 6 and Table 1), similar to Cyt WT.[2,8,32] Notably, grouping the slow kinetic component decays from C10 and C15 together with the C5 component yields an exponential decay in the entire range of chain lengths explored. The tunneling decay parameter determined from this variation is ca. 0.8 per $-CH_2-$ group which, considering the errors involved in the measurements and data processing, is compatible with the average value of 1.1 reported in the literature for electron tunneling across SAMs of alkanethiols.[36−38]

Note that, on average, the experimentally determined fast and slow ET kinetic components differ by about a factor of 22 (Table 1), in excellent agreement with the differences predicted from MD simulations and pathways calculations between high- and low-affinity K87C/SAM electrostatic complexes (see above).

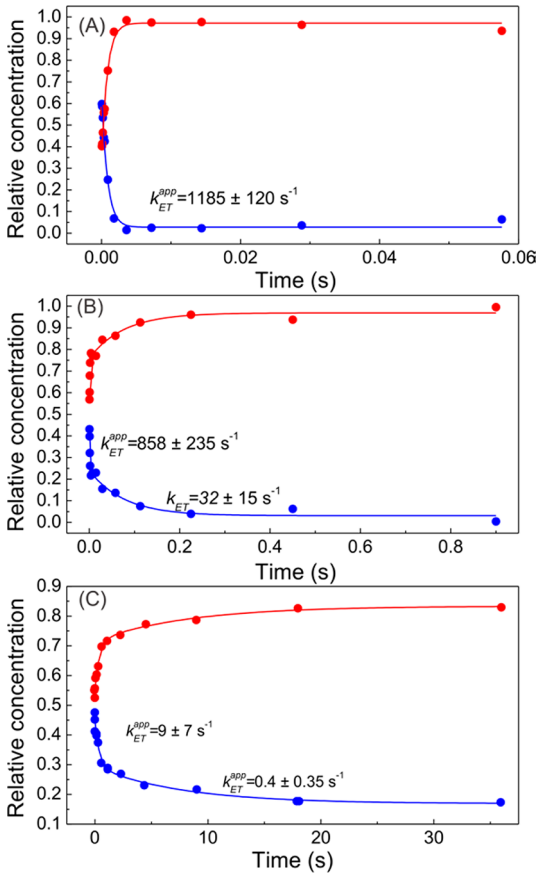

Figure 5. Representative kinetics of K87C reduction adsorbed on C5 (A), C10 (B), and C15 (C) SAMs as monitored by TR-SERR. The relative concentrations of ferrous and ferric Cyt are shown in red and blue, respectively. While monophasic kinetics are observed on C5, reproducible biphasic curves are obtained for both C10 and C15. Fitting to biexponential functions allows for disentanglement of the fast and slow contributions to the of the ET rate.

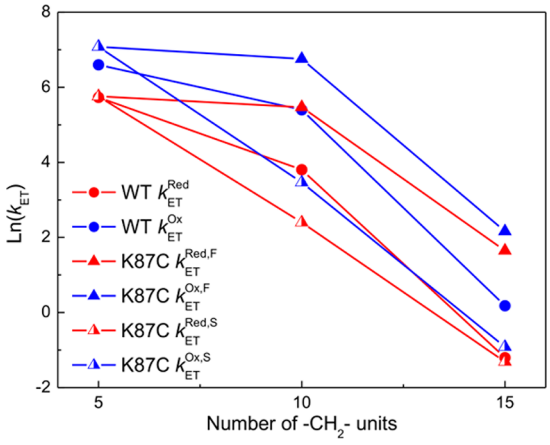

Figure 6. Distance dependence of k_{ET}^{app} for both the oxidation (red) and reduction (blue) processes of Cyt WT (circles) and K87C (triangles). Full and half-filled triangles represent the fast and slow component of k_{ET}^{app} for K87C, respectively.

Experimental and computational results obtained here display a consistent overall picture. At thicker SAMs, which also correspond to weaker interfacial electric fields,[24,32,39] low- and high-amplitude motions of adsorbed WT ferric Cyt and of interfacial water molecules are expected to be significantly faster

dx.doi.org/10.1021/jp400832m | J. Phys. Chem. B 2013, 117, 6061−6068

than electron tunneling. Indeed, rotational diffusion of WT Cyt on C15-SAMs has been estimated to be at least 4 orders of magnitude faster than ET.[6] Therefore, as a result of the interplay between fast reorientation dynamics and weak electronic coupling, redox reactions are expected to occur almost exclusively from a narrow range of high coupling orientations, thus leading to monophasic kinetics.

In contrast, the biphasic kinetics of K87C at lower electric fields (C15 and C10) indicate that ET takes place from both the high-affinity *and* the low-affinity orientations. This behavior can be rationalized in terms of the factors that control the strength of Cyt binding to the SAM-coated electrode, which are the local binding energy in the absence of an external electric field as it is estimated by the MD simulations, and the contributions due to the external electric field that are determined by the electrode potential and, thus, are not directly accessible by the present theoretical approach. However, some insight about the importance of the latter contribution is gained when considering the alignment of protein dipole moments with the interfacial electric fields, which are nearly parallel for the orientations of K87C in the low-affinity binding zone. Consequently, transitions from this binding zone, associated with low electronic couplings, to the high-affinity binding zone might be slower than reorientation dynamics of the WT protein, resulting in a biphasic ET kinetics for thick SAMs (C10 and C15). As the strength of the interfacial electric field increases, those orientations that lead to a good alignment of the dipole moment but relatively weak coupling are strongly favored, as reflected by the monophasic kinetics on thin films (C5). This interpretation suggests that on C5, only the slow kinetic component is probed experimentally, which is supported by the recovery of the exponential distance dependence when only considering such component in the entire length range explored.

CONCLUSIONS

Since the first reports describing the anomalous distance dependencies of protein ET on SAM-coated electrodes, many possible explanations were suggested, such as (i) a transition from a nonadiabatic to an adiabatic regime,[40] (ii) a two-states model, comprising redox active and inactive states,[2,9] and (iii) a gating mechanism involving protein reorientation.[6] Though we have previously reported evidence in favor of protein dynamics constituting the rate-limiting step at short lengths (or strong electric fields),[6,12,41] some fundamental issues remained unaddressed, such as the absence of an electrochemical response from both the high and low coupling regions. Of great significance, the exponential distance dependence of k_{ET} was recovered by disentangling protein dynamics from ET kinetics. This was achieved by rational surface mutations that change the energetic balance of the Cyt−SAM complexes, allowing us to confirm here our previous hypothesis, thus emphasizing the role of interfacial electric fields in modulating the interplay between protein dynamics and electron tunneling.

ASSOCIATED CONTENT

Supporting Information

Additional computational and spectroelectrochemical results are provided as Supporting Information. This material is available free of charge via the Internet at http://pubs.acs.org.

AUTHOR INFORMATION

Corresponding Author

*E-mail: hildebrandt@chem.tu-berlin.de (P.H.); dhmurgida@qi.fcen.uba.ar (D.H.M.).

Author Contributions

⊥These authors contributed equally.

Notes

The authors declare no competing financial interest.

ACKNOWLEDGMENTS

Financial support by ANPCyT (PICT 2010-070 and 2011-1249), UBA (UBACyT 20020090100094) and the DFG (Cluster of Excellence) is gratefully acknowledged. Computer simulations were performed using resources kindly provided by the Open Science Grid, which is supported by the National Science Foundation and the U.S. Department of Energy's Office of Science.

REFERENCES

(1) Gray, H. B.; Winkler, J. R. Electron Transfer in Proteins. *Annu. Rev. Biochem.* **1996**, *65*, 537−561.

(2) Avila, A.; Gregory, B. W.; Niki, K.; Cotton, T. M. An Electrochemical Approach to Investigate Gated Electron Transfer Using a Physiological Model System: Cytochrome *c* Immobilized on Carboxylic Acid-terminated Alkanethiol Self-assembled Monolayers on Gold Electrodes. *J. Phys. Chem. B* **2000**, *104*, 2759−2766.

(3) Chi, Q. J.; Zhang, J. D.; Andersen, J. E. T.; Ulstrup, J. Ordered Assembly and Controlled Electron Transfer of the Blue Copper Protein Azurin at Gold (111) Single-Crystal Substrates. *J. Phys. Chem. B* **2001**, *105*, 4669−4679.

(4) Davis, K. L.; Waldeck, D. H. Effect of Deuterium Substitution on Electron Transfer at Cytochrome-SAM interfaces. *J. Phys. Chem. B* **2008**, *112*, 12498−12507.

(5) El Kasmi, A.; Wallace, J. M.; Bowden, E. F.; Binet, S. M.; Linderman, R. J. Controlling Interfacial Electron-Transfer Kinetics of Cytochrome *c* With Mixed Self-assembled Monolayers. *J. Am. Chem. Soc.* **1998**, *120*, 225−226.

(6) Kranich, A.; Ly, H. K.; Hildebrandt, P.; Murgida, D. H. Direct Observation of the Gating Step in Protein Electron Transfer: Electric-field-controlled Protein Dynamics. *J. Am. Chem. Soc.* **2008**, *130*, 9844−9848.

(7) Molinas, M. F.; De Candia, A.; Szajnman, S. H.; Rodríguez, J. B.; Martí, M.; Pereira, M.; Teixeira, M.; Todorovic, S.; Murgida, D. H. Electron Transfer Dynamics of *Rhodothermus marinus caa*$_3$ Cytochrome *c* Domains on Biomimetic Films. *Phys. Chem. Chem. Phys.* **2011**, *13* (40), 18088−18098.

(8) Murgida, D. H.; Hildebrandt, P. Proton-Coupled Electron Transfer of Cytochrome *c*. *J. Am. Chem. Soc.* **2001**, *123*, 4062−4068.

(9) Niki, K.; Hardy, W. R.; Hill, M. G.; Li, H.; Sprinkle, J. R.; Margoliash, E.; Fujita, K.; Tanimura, R.; Nakamura, N.; Ohno, H.; Richards, J. H.; Gray, H. B. Coupling to Lysine-13 Promotes Electron Tunneling Through Carboxylate-terminated Alkanethiol Self-assembled Monolayers to Cytochrome *c*. *J. Phys. Chem. B* **2003**, *107*, 9947−9949.

(10) Wei, J. J.; Liu, H. Y.; Khoshtariya, D. E.; Yamamoto, H.; Dick, A.; Waldeck, D. H. Electron-transfer Dynamics of Cytochrome *c*: A Change in the Reaction Mechanism with Distance. *Angew. Chem., Int. Ed.* **2002**, *41* (24), 4700−4703.

(11) Xu, J. S.; Bowden, E. F. Determination of the Orientation of Adsorbed Cytochrome *c* on Carboxyalkanethiol Self-assembled Monolayers by *in situ* Differential Modification. *J. Am. Chem. Soc.* **2006**, *128*, 6813−6822.

(12) Alvarez Paggi, D.; Martin, D. F.; De Biase, P. M.; Hildebrandt, P.; Marti, M. A.; Murgida, D. H. Molecular Basis of Coupled Protein and Electron Transfer Dynamics of Cytochrome *c* in Biomimetic Complexes. *J. Am. Chem. Soc.* **2010**, *132*, 5769−5778.

(13) Lange, C.; Hunte, C. Crystal Structure of the Yeast Cytochrome bc_1 Complex with its Bound Substrate Cytochrome *c*. *Proc. Natl. Acad. Sci. U.S.A.* **2002**, *99* (5), 2800−2805.
(14) Pelletier, H.; Kraut, J. Crystal Structure of a Complex Between Electron Transfer Partners, Cytochrome *c* Peroxidase and Cytochrome *c*. *Science* **1992**, *258* (5089), 1748−1755.
(15) Roberts, V. A.; Pique, M. E. Definition of the Interaction Domain for Cytochrome *c* on Cytochrome *c* Oxidase. III. Prediction of the Docked Complex by a Complete, Systematic Search. *J. Biol. Chem.* **1999**, *274* (53), 38051−38060.
(16) Lao, K.; Franzen, S.; Steffen, M.; Lambright, D.; Stanley, R.; Boxer, S. G. Effects of Applied Electric Fields on the Quantum Yields for the Initial Electron Transfer Steps in Bacterial Photosynthesis II. Dynamic Stark Effect. *Chem. Phys.* **1995**, *197* (3), 259−275.
(17) Pudlak, M.; Pincak, R. Influence of the Electric Field on the Electron Transport in Photosynthetic Reaction Centers. *Eur. Phys. J. E* **2011**, *34* (3), 1−8.
(18) Kim, Y. C.; Furchtgott, L. A.; Hummer, G. Biological Proton Pumping in an Oscillating Electric Field. *Phys. Rev. Lett.* **2009**, *103* (26), 268102−268112.
(19) Abriata, L. A.; Álvarez-Paggi, D.; Ledesma, G. N.; Blackburn, N. J.; Vila, A. J.; Murgida, D. H. Alternative Ground States Enable Pathway Switching in Biological Electron Transfer. *Proc. Natl. Acad. Sci. U.S.A.* **2012**, *109* (43), 17348−17353.
(20) Feng, J. J.; Hildebrandt, P.; Murgida, D. H. Silver Nanocoral Structures on Electrodes: A Suitable Platform for Protein-based Bioelectronic Devices. *Langmuir* **2008**, *24*, 1583−1586.
(21) Willner, B.; Katz, E.; Willner, I. Electrical Contacting of Redox Proteins by Nanotechnological Means. *Curr. Opin. Biotechnol.* **2006**, *17* (6), 589−596.
(22) Tenger, K.; Khoroshyy, P.; Kovács, K. L.; Zimányi, L.; Rákhely, G. Improved System for Heterologous Expression of Cytochrome *c* Mutants in *Escherichia coli*. *Acta Biol. Hung.* **2007**, *58*, 23−35.
(23) Tenger, K.; Khoroshyy, P.; Rákhely, G.; Zimányi, L. Maturation of a Eukaryotic Cytochrome *c* in the Cytoplasm of *Escherichia coli* Without the Assistance by a Dedicated Biogenesis Apparatus. *J. Bioenerg. Biomembr.* **2010**, *42* (2), 125−133.
(24) Murgida, D. H.; Hildebrandt, P. Heterogeneous Electron Transfer of Cytochrome *c* on Coated Silver Electrodes. Electric Field Effects on Structure and Redox Potential. *J. Phys. Chem. B* **2001**, *105*, 1578−1586.
(25) Dopner, S.; Hildebrandt, P.; Mauk, A. G.; Lenk, H.; Stempfle, W. Analysis of Vibrational Spectra of Multicomponent Systems. Application to pH-dependent Resonance Raman Spectra of Ferricytochrome *c*. *Spectrochim. Acta A* **1996**, *52* (5), 573−584.
(26) Bryant, M. A.; Pemberton, J. E. Surface Raman Scattering of Self-assembled Monolayers Formed From 1-alkanethiols at Silver Electrodes. *J. Am. Chem. Soc.* **1991**, *113*, 3629−3637.
(27) Bushnell, G. W.; Louie, G. V.; Brayer, G. D. High-resolution Three-dimensional Structure of Horse Heart Cytochrome *c*. *J. Mol. Biol.* **1990**, *214* (2), 585−595.
(28) Rai, B.; Sathish, P.; Malhotra, C. P.; Pradip; Ayappa, K. G. Molecular Dynamic Simulations of Self-assembled Alkylthiolate Monolayers on an Au(111) Surface. *Langmuir* **2004**, *20*, 3138−3144.
(29) Beratan, D. N.; Onuchic, J. N.; Winkler, J. R.; Gray, H. B. Electron-tunneling Pathways in Proteins. *Science* **1992**, *258* (5089), 1740−1741.
(30) Koppenol, W. H.; Rush, J. D.; Mills, J. D.; Margoliash, E. The Dipole-moment of Cytochrome *c*. *Mol. Biol. Evol.* **1991**, *8* (4), 545−558.
(31) Paggi, D. A.; Martin, D. F.; Kranich, A.; Hildebrandt, P.; Marti, M. A.; Murgida, D. H. Computer Simulation and SERR Detection of Cytochrome *c* Dynamics at SAM-coated Electrodes. *Electrochim. Acta* **2009**, *54* (22), 4963−4970.
(32) Murgida, D. H.; Hildebrandt, P. Electron-transfer Processes of Cytochrome *c* at Interfaces. New Insights by Surface-enhanced Resonance Raman Spectroscopy. *Acc. Chem. Res.* **2004**, *37*, 854−861.
(33) Wallace, C. J.; Proudfoot, A. E. On the Relationship Between Oxidation-Reduction Potential and Biological Activity in Cytochrome *c* Analogues. Results From Four Novel Two-Fragment Complexes. *Biochem. J.* **1987**, *245* (3), 773−779.
(34) Oellerich, S.; Wackerbarth, H.; Hildebrandt, P. Spectroscopic Characterization of Nonnative Conformational States of Cytochrome *c*. *J. Phys. Chem. B* **2002**, *106*, 6566−6580.
(35) Getz, E. B.; Xiao, M.; Chakrabarty, T.; Cooke, R.; Selvin, P. R. A Comparison Between the Sulfhydryl Reductants Tris (2-carboxyethyl) Phosphine and Dithiothreitol for Use in Protein Biochemistry. *Anal. Biochem.* **1999**, *273* (1), 73−80.
(36) Finklea, H. O.; Hanshew, D. D. Electron-Transfer Kinetics in Organized Thiol Monolayers with Attached Pentaammine (Pyridine) Ruthenium Redox Centers. *J. Am. Chem. Soc.* **1992**, *114*, 3173−3181.
(37) Xu, J.; Li, H.; Zhang, Y. Relationship Between Electronic Tunneling Coefficient and Electrode Potential Investigated by Using Self-assembled Alkanethiol Monolayers on Gold Electrodes. *J. Phys. Chem.* **1993**, *97*, 11497−11500.
(38) Smalley, J. F.; Feldberg, S. W.; Chidsey, C. E. D.; Linford, M. R.; Newton, M. D.; Liu, Y. P. The Kinetics of Electron Transfer through Ferrocene-terminated Alkanethiol Monolayers on Gold. *J. Phys. Chem.* **1995**, *99*, 13141−13149.
(39) Smith, C. P.; White, H. S. Theory of the Interfacial Potential Distribution and Reversible Voltammetric Response of Electrodes Coated with Electroactive Molecular Films. *Anal. Chem.* **1992**, *64*, 2398−2405.
(40) Yue, H. J.; Khoshtariya, D.; Waldeck, D. H.; Grochol, J.; Hildebrandt, P.; Murgida, D. H. On the Electron Transfer Mechanism Between Cytochrome *c* and Metal Electrodes. Evidence for Dynamic Control at Short Distances. *J. Phys. Chem. B* **2006**, *110*, 19906−19913.
(41) Ly, H. K.; Marti, M. A.; Martin, D. F.; Alvarez-Paggi, D.; Meister, W.; Kranich, A.; Weidinger, I. M.; Hildebrandt, P.; Murgida, D. H. Thermal Fluctuations Determine the Electron-Transfer Rates of Cytochrome *c* in Electrostatic and Covalent Complexes. *ChemPhysChem* **2010**, *11* (6), 1225−1235.

Supporting Information

Disentangling Electron Tunneling and Protein Dynamics of Cytochrome *c* Through a Rationally Designed Surface Mutation

Damián Alvarez-Paggi, Wiebke Meister, Uwe Kuhlmann, Inez Weidinger, Katalin Tenger, László Zimányi, Gábor Rákhely, Peter Hildebrandt* and Daniel H. Murgida*

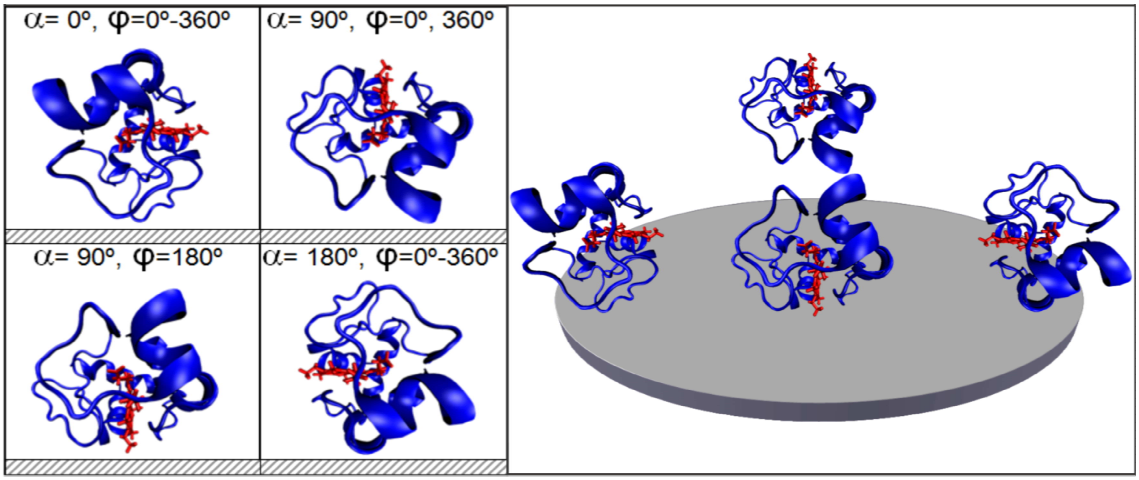

Scheme S1. Representation of the different orientations of the Cyt-SAM complexes for key α and φ values (left) and their corresponding positions in the α vs φ plots.

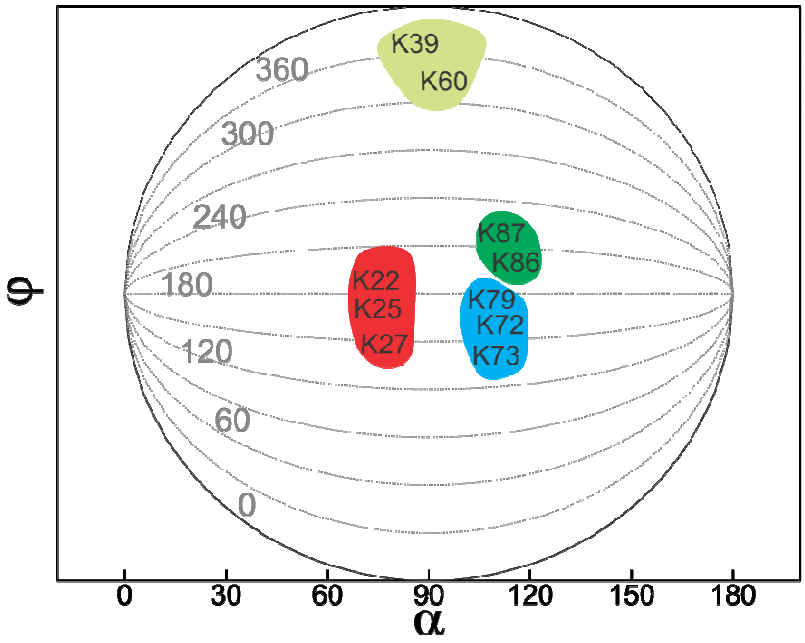

Figure S1. Representation of the key lysine (K) residues that establish Cyt-SAM contacts in the different orientations defined by the α and φ angles. Comparison with Figure 3 shows that K87 stabilizes Cyt in orientations that exhibit a low average electronic coupling. Further details regarding lysine residues and their role in the complex formation may be found elsewhere.[1,2]

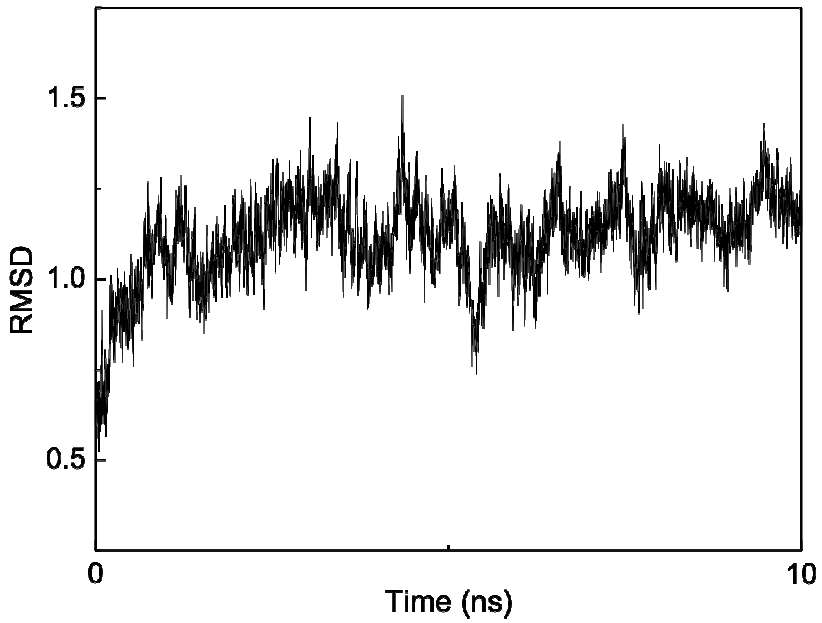

Figure S2. RMSD of the backbone structure of K87C for a 10 ns thermalization MD. The RMSD value is below 1.5 Å, indicative of a preserved protein folding.

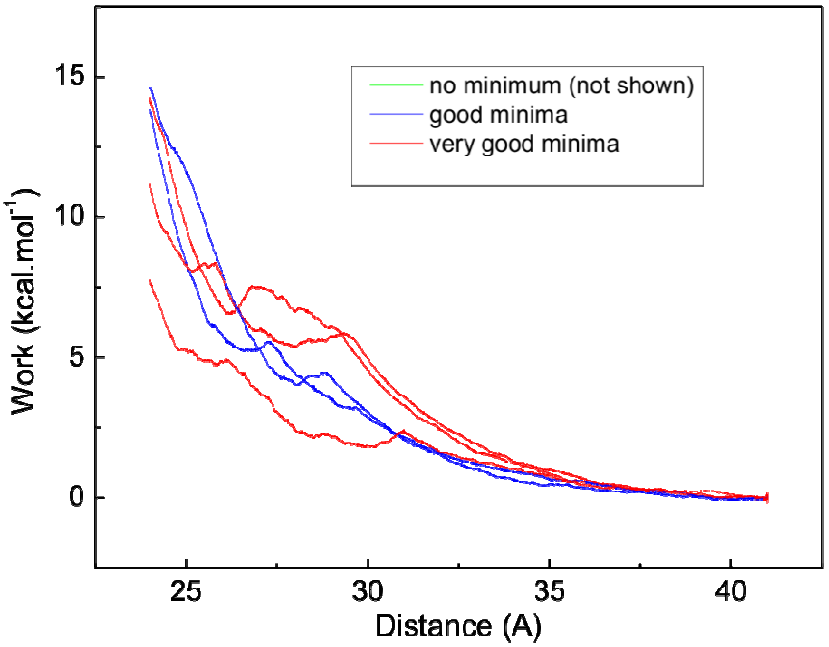

Figure S3. Work-vs-distance profiles from the SMD simulations of K87C. The trajectories that yielded an energy minimum are displayed. The structures corresponding to said minima were employed as starting point for the MD simulations in explicit solvent.

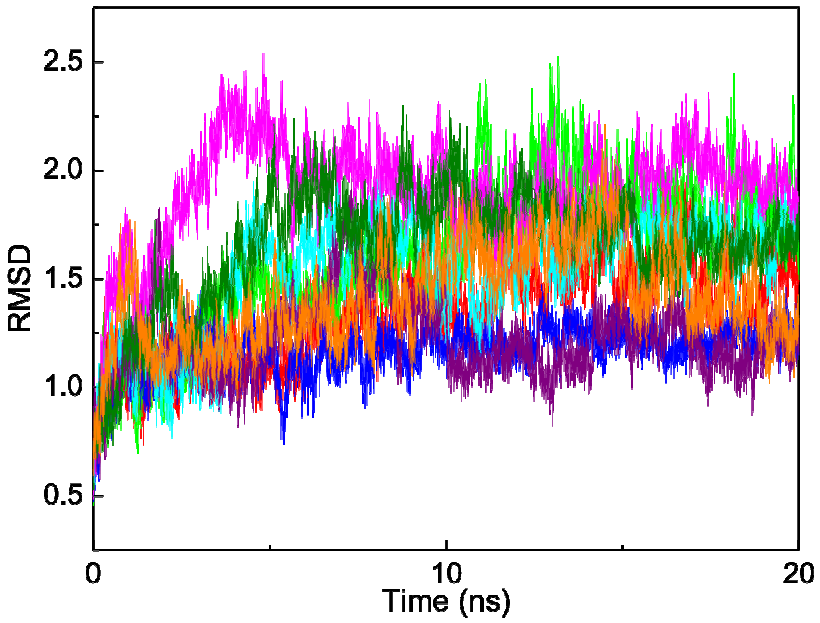

Figure S4. RMSD plots for the 20 ns MD simulations of K87C adsorbed on SAMs in explicit solvent. Each color represents a different trajectory. In every case the RMSD value is below 2.5 Å, indicative of a preserved protein folding.

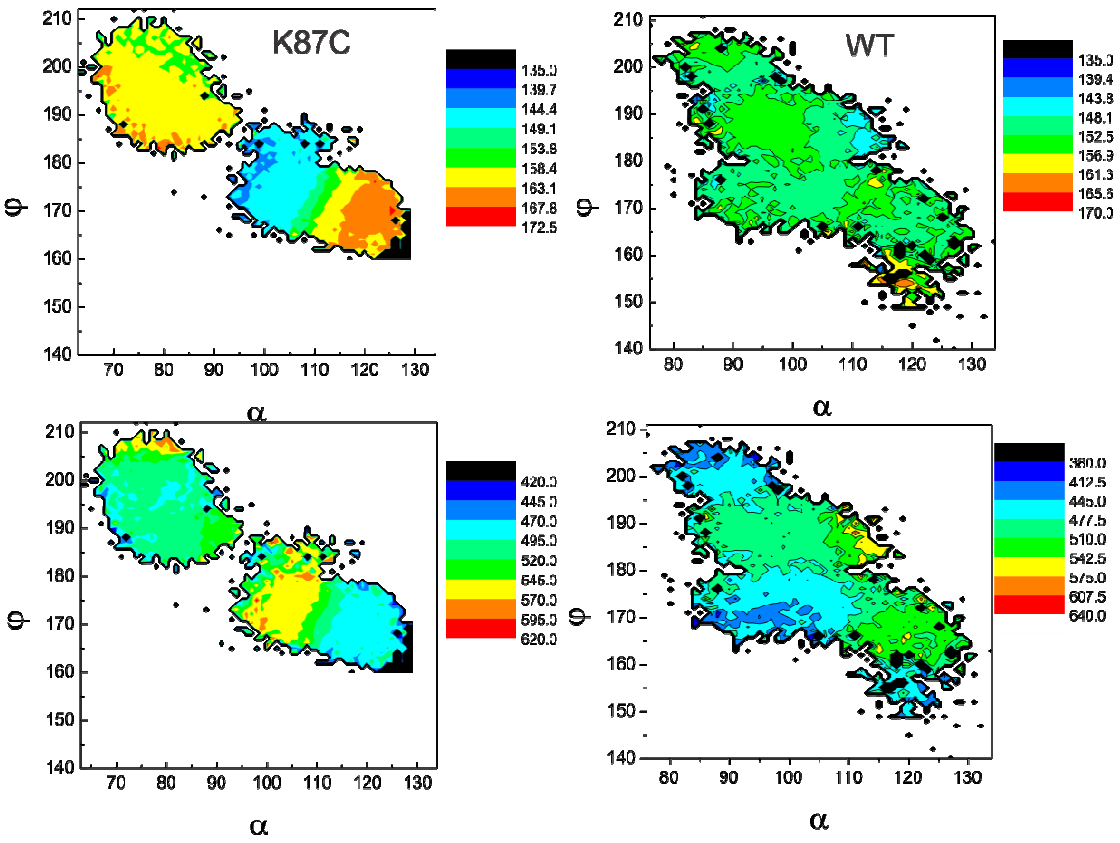

Figure S5. Dipole moment orientation vs *Z* axis (top) and modulus (bottom) for K87C (left) and WT Cyt variants (right) as a function of the orientational angles α and φ.

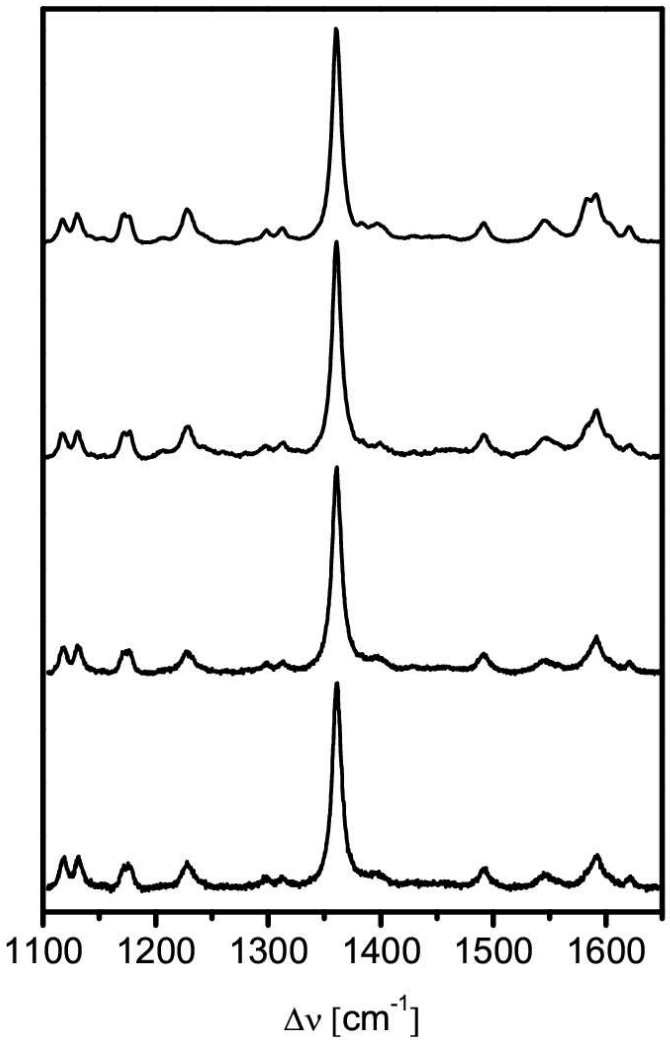

Figure S6. Comparison of SERR spectra of ferrous Cyt on a C10-SAM coated Ag electrode at -0.4 V with the RR spectra of ferrous WT Cyt and K87C. From top to bottom: RR spectrum of the WT Cyt, RR spectrum of K87C, SERR spectrum of the WT Cyt, SERR spectrum of K87C. Spectra were measured with 413 nm excitation. Reduction of the proteins in solution was achieved chemically by adding dithionite. Potentials refer to the Ag/AgCl (3M KCl) reference electrode.

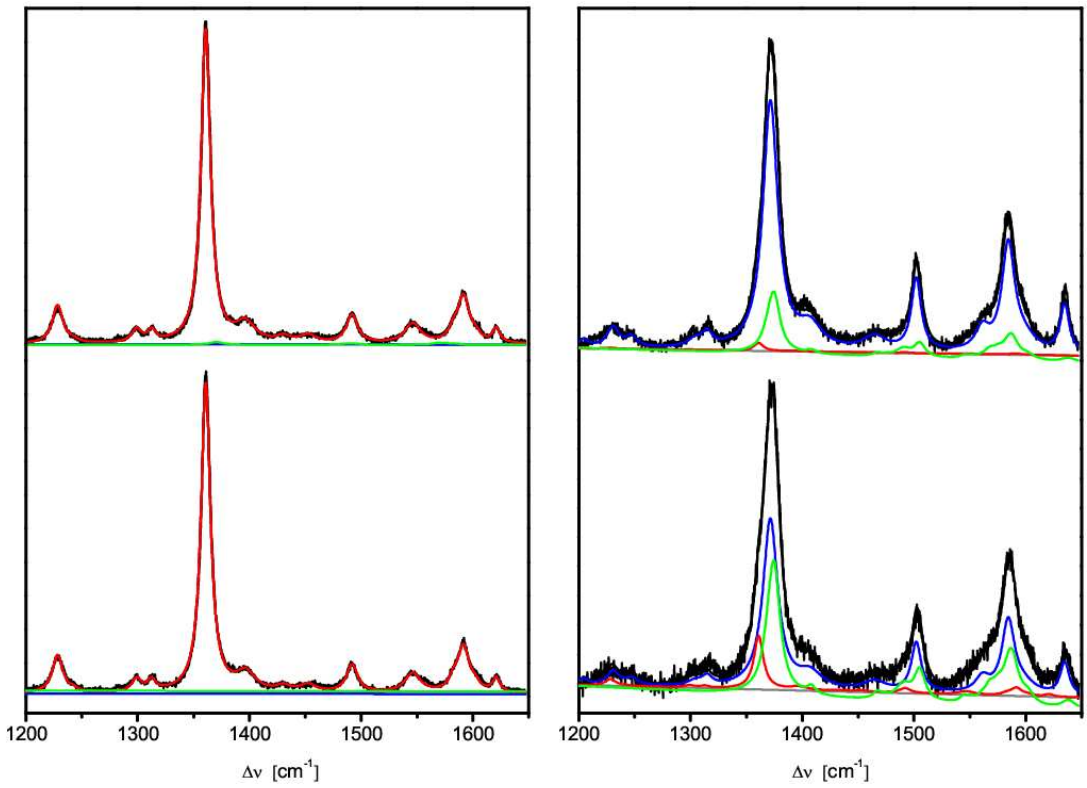

Figure S7A. SERR experimental spectra of WT Cyt (top) and K87C (bottom) on a C5-SAM coated electrode measured at -400 mV (left) and +150 mV (right) with 413 nm excitation. The component spectra of ferric B1, ferrous B1, and ferric B2 (HS and LS) are represented by the blue, red, and green lines. The baseline is displayed in grey and the overall fit (sum of the component spectra) is shown on black.

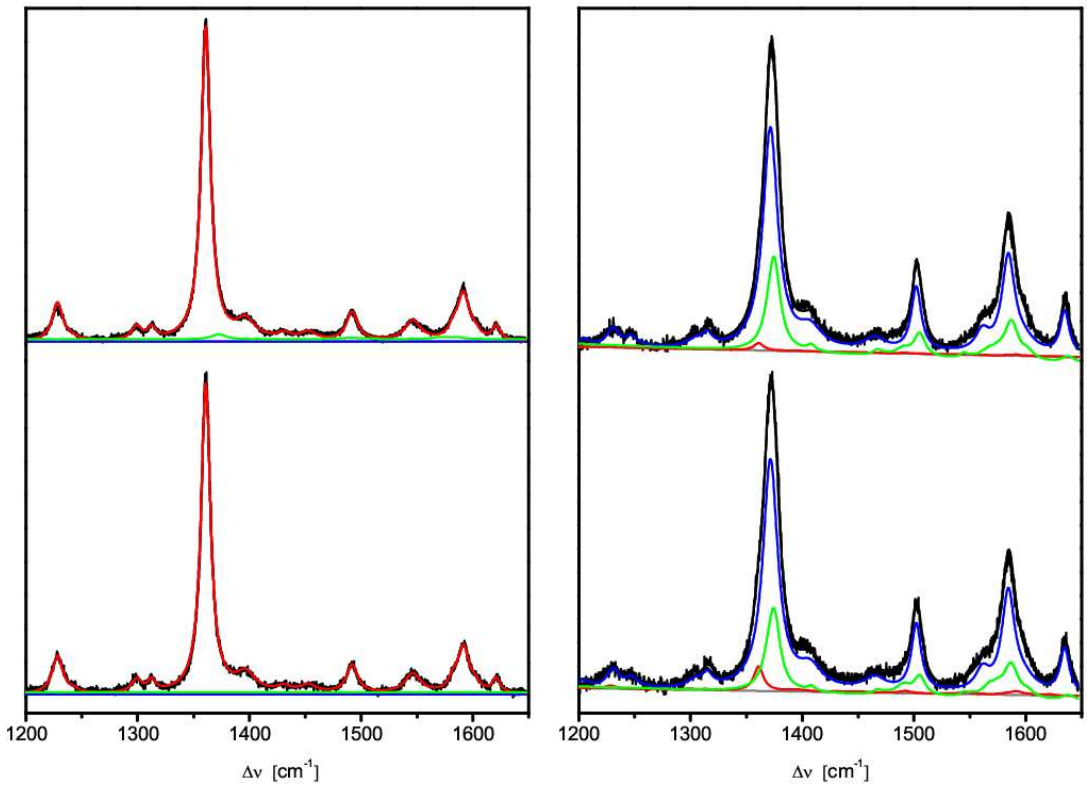

Figure S7B. SERR experimental spectra of WT Cyt (top) and K87C (bottom) on a C10-SAM coated electrode measured at -400 mV (left) and +150 mV (right) with 413 nm excitation. The component spectra of ferric B1, ferrous B1, and ferric B2 (HS and LS) are represented by the blue, red, and green lines. The baseline is displayed in grey and the overall fit (sum of the component spectra) is shown on black.

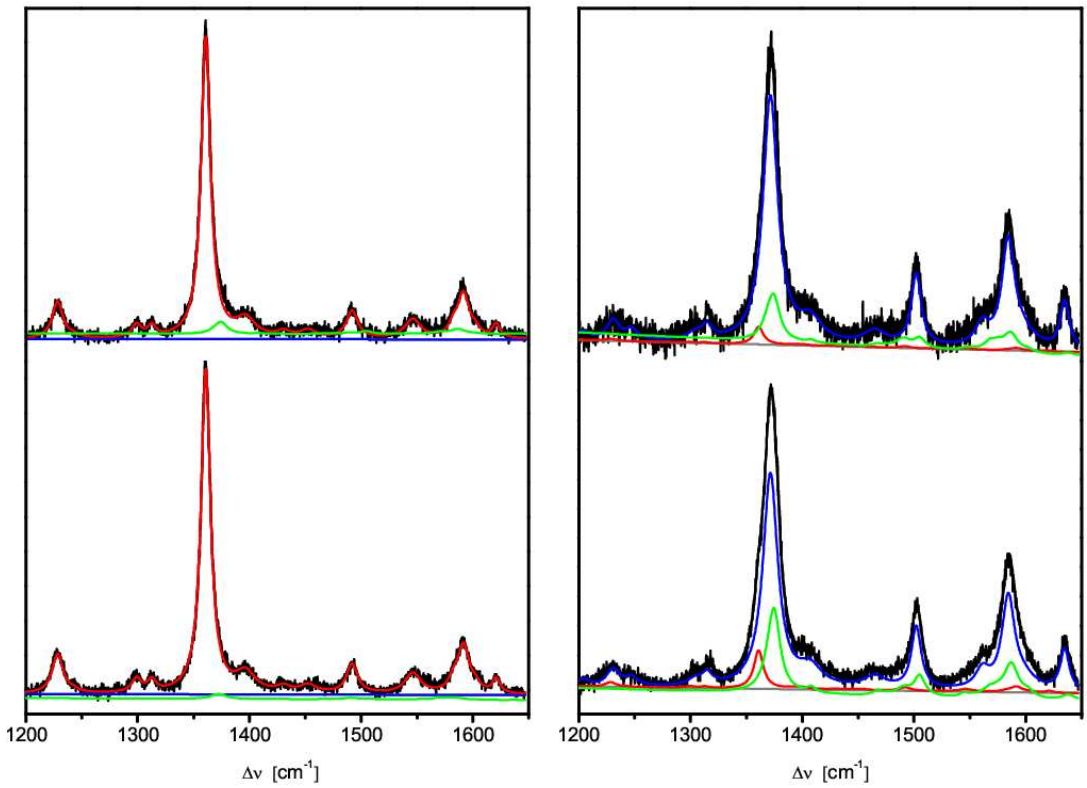

Figure S7C. SERR experimental spectra of WT Cyt (top) and K87C (bottom) on a C15-SAM coated electrode measured at -400 mV (left) and +150 mV (right) with 413 nm excitation. The component spectra of ferric B1, ferrous B1, and ferric B2 (HS and LS) are represented by the blue, red, and green lines. The baseline is displayed in grey and the overall fit (sum of the component spectra) is shown on black.

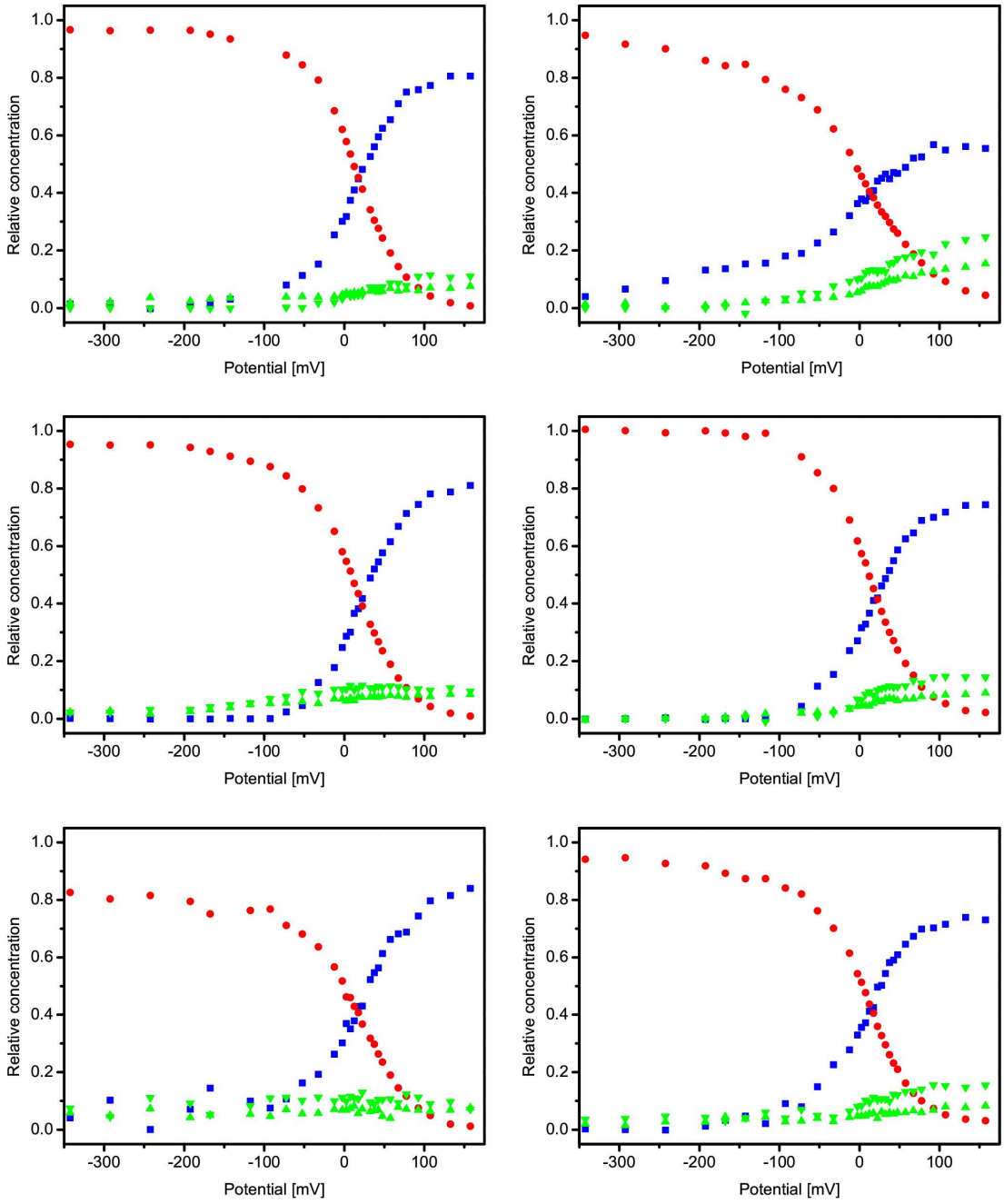

Figure S8. Potential dependence of the relative concentrations of the various Cyt species as derived from the component analysis of the experimental SERR spectra of WT Cyt (left) and K87C (right) on C5 (top), C10 (middle) and C15 (bottom) SAMs. The red circles and blue squares refer to the reduced and oxidized B1 species, respectively. The non-native oxidized B2 species are presented by green triangles (high spin – upright; low spin – reversed).

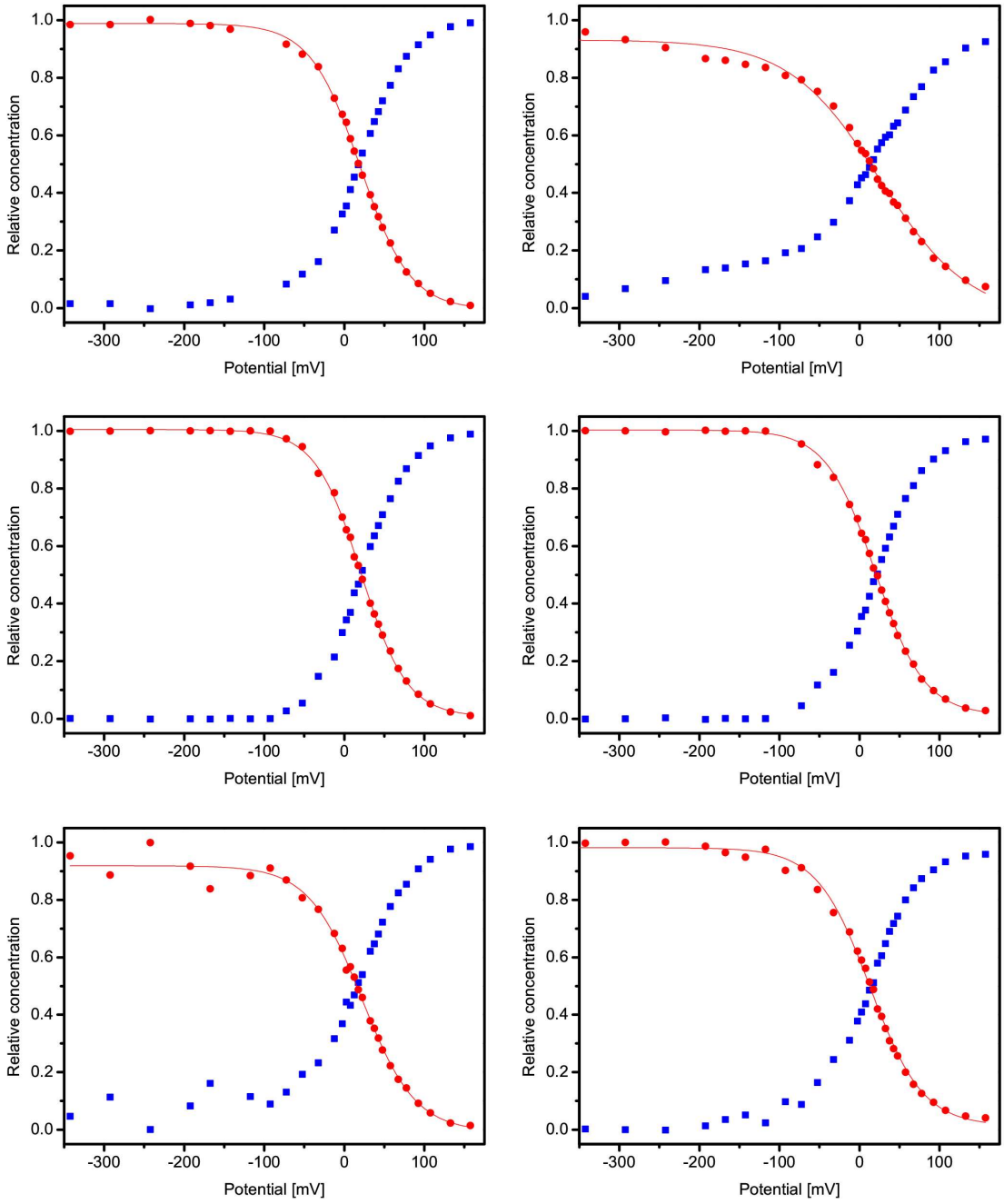

Figure S9. Nernst plots derived from the component analysis of the stationary experimental SERR spectra of the WT Cyt (left) and K87C (right) on C5 (top), C10 (middle) and C15 (bottom) SAMs. The red circles and blue squares refer to the reduced and oxidized B1 species, respectively.

References

(1) Alvarez Paggi, D.; Martin, D. F.; De Biase, P. M.; Hildebrandt, P.; Marti, M. A.; Murgida, D. H. Molecular Basis of Coupled Protein and Electron Transfer Dynamics of Cytochrome *c* in Biomimetic Complexes. *J. Am. Chem. Soc.* **2010**, *132* (16), 5769-5778 .
(2) Paggi, D. A.; Martin, D. F.; Kranich, A.; Hildebrandt, P.; Marti, M. A.; Murgida, D. H. Computer Simulation and SERR Detection of Cytochrome *c* Dynamics at SAM-coated Electrodes. *Electrochim. Acta* **2009,** *54* (22), 4963-4970.